Pergamon

Cement and Concrete Research 29 (1999) 705–712

CEMENT AND CONCRETE RESEARCH

Fatigue crack growth of high-strength concrete in wedge-splitting test

Jin-Keun Kim [a,*], Yun-Yong Kim [b]

[a] *Department of Civil Engineering, Korea Advanced Institute of Science and Technology, Kusong 373-1, Yusong, Taejon, Korea*

[b] *Railway Division, Chungsuk Engineering Co., Ltd., Seocho-1 1606-1, Seocho, Seoul, Korea*

Manuscript received 11 March 1998; accepted manuscript 29 January 1999

Abstract

In this study, a wedge-splitting testing was carried out for the investigation of fatigue crack growth behavior of high strength concrete. Selected test variables were concrete compressive strength (28, 60, and 118 MPa) and stress ratio (6, 13%). In order to apply the target stress ratio, the maximum and the minimum fatigue loadings were 75–85 and 5–10% of ultimate static load, respectively. Fatigue testing was preceded by crack mouth opening displacement (CMOD) compliance calibration, and then the fatigue crack growth was computed by crack length vs. the CMOD compliance relations acquired by the CMOD compliance calibration technique. In the fatigue test, the frequency of loading cycle was 1 Hz, and the initial notch length a_0 was 30% of specimen height. To verify the applicability of the CMOD compliance calibration technique to wedge-splitting testing, the crack lengths measured by this method were compared with those predicted by linear elastic fracture mechanics (LEFM) and dye penetration testing. On the basis of the experimental results, an LEFM-based empirical model for fatigue crack growth rate ($da/dn - \Delta K_I$ relationship) that takes strength into account was suggested. The fatigue crack growth rate increased with the strength of concrete. It appeared that the $da/dN - \Delta K_I$ relationship depended on stress ratio, and the effect was evaluated by the proposed equation. In addition, the comparisons between the CMOD compliance calibration technique and the other methods supported the validity of this technique in the wedge splitting test.

Keywords: Fatigue; Fatigue crack growth rate; Wedge-splitting test; CMOD compliance calibration technique; Dye penetration test

In recent years, interest has risen concerning the behavior of high-strength concrete subjected to fatigue loading because of its frequent use in structures such as long-span bridges, offshore structures, and reinforced concrete pavements. Fatigue is a process of progressive and permanent internal damage in a material subjected to repeated loading. This is attributed to the propagation of internal microcracks that may result in the growth of cracks and an unpredictable failure.

Fatigue failure consists of three stages: stage 1 is the crack initiation; stage 2 is the crack propagation; and stage 3 is the final failure. In the early 1960s, Paris and Erdogan [1] demonstrated that fracture mechanics is a useful tool for characterizing crack propagation by fatigue, that is to say, stage 2. The conceptual form of the crack growth model based on linear elastic fracture mechanics (LEFM) is given by Eq. (1):

$$\frac{da}{dN} = f(\Delta K, R) \tag{1}$$

where ΔK and R are stress intensity range ($K_{max} - K_{min}$) and stress ratio ($\sigma_{min}/\sigma_{max}$), respectively, and da/dN is the crack growth per cycle. A number of expressions for $f(\Delta K, R)$ have been proposed, most of which are empirical. Eq. (1) can be integrated to estimate fatigue life of which the number of cycles required to propagate a crack from an initial length a_i to a final length a_f, as shown in Eq. (2):

$$N = \int_{a_i}^{a_f} \frac{da}{f(\Delta K, R)} \tag{2}$$

Paris and Erdogan [1] discovered that function $f(\Delta K,R)$ takes the form of a power law that is called Paris' law as shown in Eq. (3).

$$\frac{da}{dN} = C\,\Delta K^m \tag{3}$$

C is a material constant dependent on stress ratio (R); m is also a material constant. Walker [2] proposed the following relationship [Eq. (4)] used to compensate for stress ratio, which is the so-called Walker's law.

$$\frac{da}{dN} = \frac{C\,\Delta K^m}{(1-R)^n} \tag{4}$$

in which n is an empirical constant for stress ratio and C and m are material constants that do not have the same numerical values as in Paris' law.

* Corresponding author. Tel.: 82-42-869-3614; Fax: 82-42-869-3610; E-mail: kimjinkeun@cais.kaist.ac.kr.

0008-8846/99/$–see front matter
PII: S0008-8846(99)00025-3

Table 1
Test variables

Stress ratio R (P_{min}/P_{max}, %)	Concrete strength f'_c (MPa)
6, 13	28 (LS), 60 (MS), 118 (HS)

In the 1980s, Baluch and colleagues [3] and Perdikaris and Calomino [4] reported that Paris' law is a useful method for characterizing the fatigue crack growth behavior of concrete. Works by Bazant and colleagues [5,6] that used the size effect law resulted in a modified, size adjusted Paris' law. Zhang et al. [7] used Forman's law [8] to represent the decline of stiffness by fatigue. The effect of concrete strength, however, has escaped attention.

The main objectives of the present study are to investigate the influence of concrete strength on fatigue crack growth behavior and to provide more fatigue crack growth data. The other objective is to verify the suitability of the crack mouth opening displacement (CMOD) compliance calibration technique to monitor crack growth in wedge splitting specimens. To find out the validity of the CMOD compliance calibration technique, the compliances measured by this method were compared with those predicted by the LEFM and dye penetration tests.

1. Experimental program

1.1. Test variables

Generally, fatigue tests have been carried out for a given constant minimum load or for a constant stress ratio R, which is defined as the ratio of minimum to maximum load (P_{min} and P_{max} ranged from 5–10 to 71–85% of the ultimate static load P_u, respectively. Concrete strengths of three levels were selected for these tests. Frequency of loading was 1 Hz, and the fatigue loading was applied sinusoidally. In fatigue testing, the initial notch length was 60 mm; all test variables are given in Table 1.

1.2. Materials

A single source of type I portland cement was used. Crushed stone with the maximum size of 10 mm and natural river sand were used as coarse and fine aggregates, respectively. A superplasticizer with retarder, which meets ASTM C 494 requirements for type F admixture, was used in the mixture to give good workability. Silica fume produced by Elkem Microsilica Grade 940-u (powder; Elkem Materials, Norway) was also used for the high-strength concrete (HS) of 118 MPa.

1.3. Mixture proportions and concrete properties

The mixture proportions were selected to achieve an optimal balance of compressive strength and moderately high workability. Three different mixtures shown in Table 2 were designed with target strengths of 24, 60, and 110 MPa. All mixtures were prepared in 40-liter batches in a forced mixing-type mixer. The test results of compressive strength (f_2'), splitting tensile strength (f_{sp}) and elastic modulus (E_c) are given in Table 2. A total of 120 wedge-splitting test (WST) specimens were cast, of which 60, 30, and 30 specimens were used for the CMOD compliance calibration, dye penetration, and fatigue test, respectively. Six companion cylinders ($\phi 100 \times 200$ mm) for each batch were cast (i.e., three for compressive strength and three for splitting tensile strength). Four batches were cast for the each strength level, therefore, the values of f_c', f_{sp}, and E_c in Table 2 are the average values of 12 specimens.

1.4. Preparation of Specimens and Loading Device

Fig. 1 shows the geometry and size of the specimen. The initial notch was made by inserting a steel plate inside the specimen during the casting and taking the plate out after one day. Thereafter, all specimens were cured in water until the test. A 10-mm groove was made by inserting the trigonal prism at each outer side. This groove was used for guiding the crack propagation. Just before testing, each specimen was prepared for clip gauges and loading devices.

1.5. Testing Procedure

The specimen with loading devices is shown in Fig. 2. The fatigue machine used in the present study was Instron-8506 Closed-Loop Servo-Hydraulic Dynamic Materials Testing System (Instron Corp., Canton, MA, USA) of 2500-kN capacity. In order to increase the accuracy of the tests, a 200-kN capacity load cell was calibrated for this testing system and used for wedge-splitting testing.

The method of the CMOD compliance calibration for estimating crack growth in notched beams of metallic and nonmetallic materials, such as rock and concrete, has been used extensively with success. This technique consists of the following steps:

1. Make a notch at the center of specimen width. A steel plate was inserted during placing of concrete that will give a required width (1 mm in this study).
2. Attach the knife edges on the specimen by using gauge cement with acceptable stability to support the clip gauge.

Table 2
Mixture proportions and concrete properties

Mixture	C (kg/m^3)	S.F. (kg/m^3)	W (kg/m^3)	S (kg/m^3)	G (kg/m^3)	S.P. (%)	f'_c (MPa)	f_{sp} (MPa)	E_c (GPa)
LS	305	—	214	719	993	—	28.2	3.4	24.7
MS	423	—	169	606	1124	1.0	60.2	5.0	32.9
HS	565	63	140	522	1059	3.5	118.0	6.2	42.6

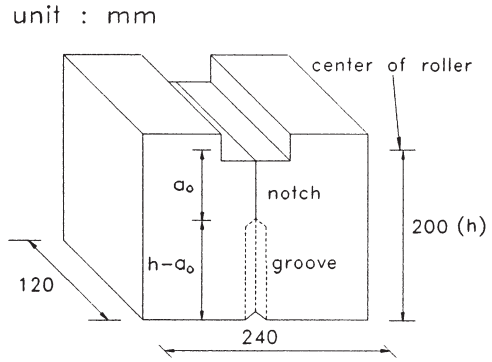

Fig. 1. Size of specimen.

3. Place the specimen in the machine and apply load. The specimens were loaded up to 30% of expected ultimate load and unloaded to zero point. This procedure was carried out three times where the average value resulted in the representative compliance value.

Selected initial notch lengths (a_0) for CMOD compliance calibration were 0.3, 0.35, 0.4, 0.45, 0.5, 0.55, and 0.6 *h*.

Dye penetration technique is a method for measuring the crack length by inserting dye into the cracked surface. Generally, a colored resin is used as a dye, of which the viscosity should be suitable for penetrating into a crack of desired width, and not for permeating the undamaged surface. In this study, the viscosity of resin was regulated to be adequate for penetrating into the visual crack, and the controlled variable during the precracking is the CMOD. The dye penetration technique was used only for verifying the validity of the CMOD compliance calibration technique because of its single usage for the same specimen. After the specimen with the initial notch length of 0.3 *h* was placed in the testing machine, the precracking and dyeing tests were carried out according to the following procedures:

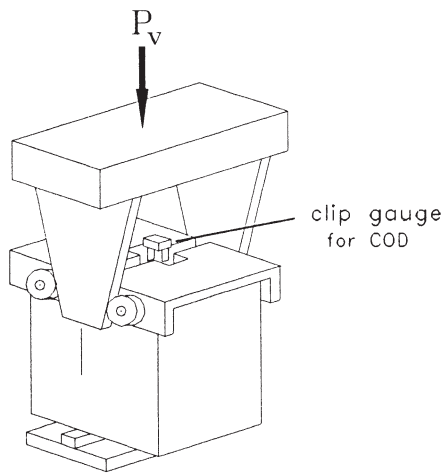

Fig. 2. Loading device of WST.

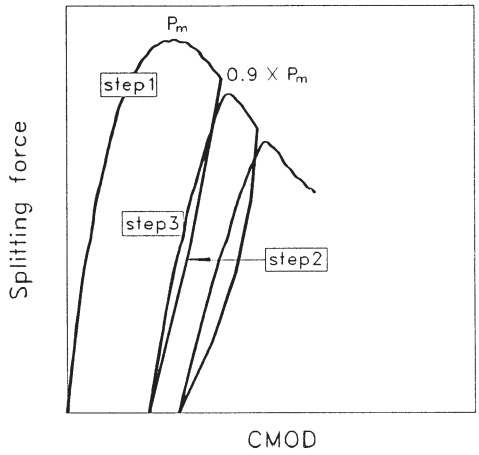

Fig. 3. Precracking procedure in dye penetration testing.

1. Using a ramping function and the CMOD control, load the specimen beyond peak load into the softening regime. Notice step 1 in Fig. 3. The load is removed at the level of about 90% of peak load as in step 2 in Fig. 3. Thereafter, the compliance is checked to see if it reaches the desired value as reference of the a_0 vs. COMD relations plotted by the CMOD compliance calibration test, which is step 3 in Fig. 3. These three steps are repeated until the value reaches the desired compliance.
2. Penetrate the dye. In order to allow the complete penetration of the dye, a reservoir is used for covering the expected cracked area in which the dye is placed. In this study, the reservoir was made of a silicone sealant.
3. Remove the dye and the reservoir. Thereafter the specimen is air-dried for 30 minutes.

The compliance of this precracked specimen was determined by means of the above-mentioned procedure of the CMOD compliance calibration technique, and then the specimen was tested until failure. After failing the specimen, the area of the dyed surface was measured. The crack length was calculated as shown in Eq. (5):

$$a_{\text{dye}} = \frac{A_{\text{dye}}}{B} \tag{5}$$

in which A_{dye} is the area of dyed surface and B is the width of ligament (100 mm).

In the fatigue test, a specimen of which initial notch length was 0.3 *h* was tested in load control at the rate of 1 Hz and the P_v − CMOD data of 10 cycles were recorded at every selected number of cycles (60, 110, or 210 cycles). The measured vertical load P_v was converted to the splitting force F_s, that is, the horizontal component of the force acting on the rollers. F_s was calculated by taking the wedge angle a into consideration according to Eq. (6):

$$F_s(= P) = \frac{P_v}{2 \times \tan \alpha} \tag{6}$$

2. Results and discussions

2.1. CMOD compliance calibration and dye penetration

The CMOD compliance calibration technique was verified by Swartz and Go [9] for plain concrete beams in bending, and also by Slowik and colleagues [10], who utilized this technique for the WST specimen. Fig. 4*(a)* shows the comparisons between test data and LEFM predictions. The measured compliance data are approximately coincident with the predicted values by LEFM. In order to apply the compliance calibration data for the fatigue analysis, regression equations of exponential form, $C = k_1 e^{n(a_0/h)}$, were fitted to the data for each concrete strength. In this equation, C is compliance, a_0/h is the ratio of initial notch length to specimen height and k_1 and n are parameters determined by regression analysis. Fig. 4*(b)* is the a/h vs. compliances relations of notched and dyed specimens. The compliances of the dyed specimens computed on the basis of Eq. (5) are roughly equivalent to those of notched specimens and similar to those of LEFM. The results of the dye penetration test verified that both the CMOD compliance technique (notched specimen) and LEFM were useful and convenient methods for predicting crack length in the wedge-splitting test.

Dyed surfaces for some specimens are shown in Fig. 5. In this figure, the measured values of a/h for low strength concrete (LS), medium strength concrete (MS), and high strength concrete (HS) are 0.432, 0.413, and 0.539, respectively. Typically, penetration depth depends on the viscosity of the dye, crack width, and diffusion time. The viscosity was determined in a preliminary test that was suitable for penetrating the width of visual crack. The penetration time in the present test was 30 minutes. Work by Swartz and Go [9] and Perdikaris and colleagues [11] indicated that the shapes of the crack fronts in beams were either parabolic or straight; however, the shapes of the crack fronts, in this study, were approximately straight lines as shown in Fig. 5.

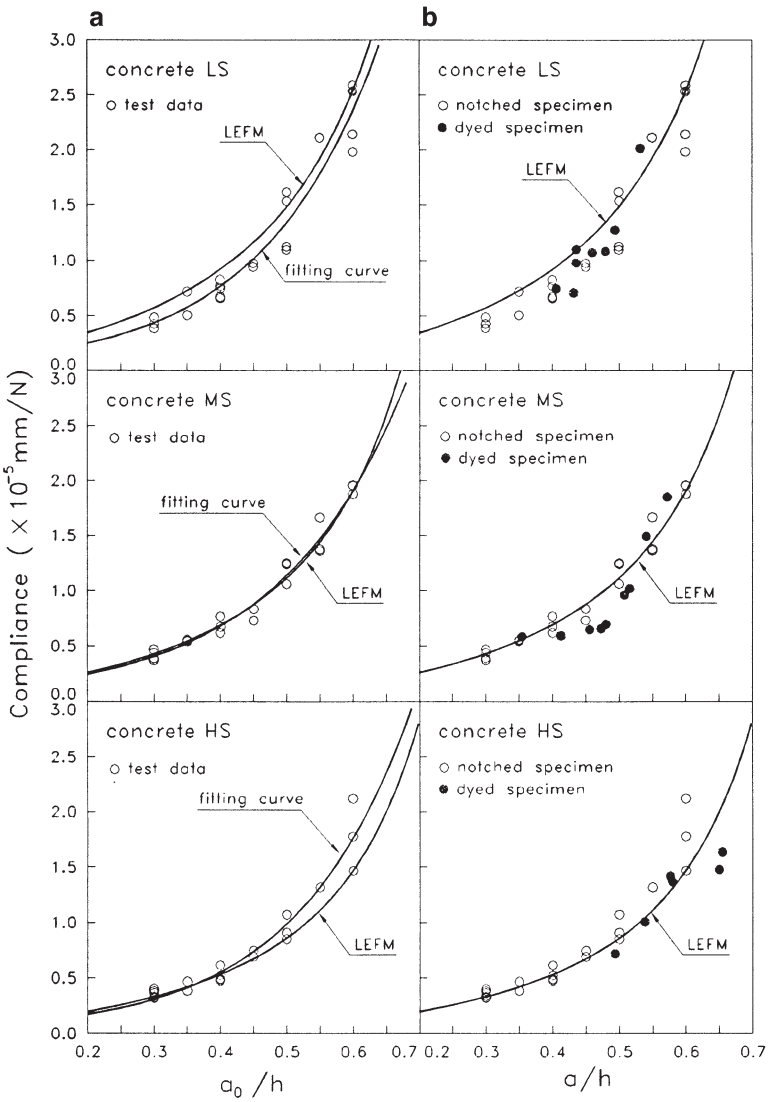

Fig. 4. CMOD compliance calibration curves. *(a)* Notched specimens with predicted curve, *(b)* notched and dyed specimens.

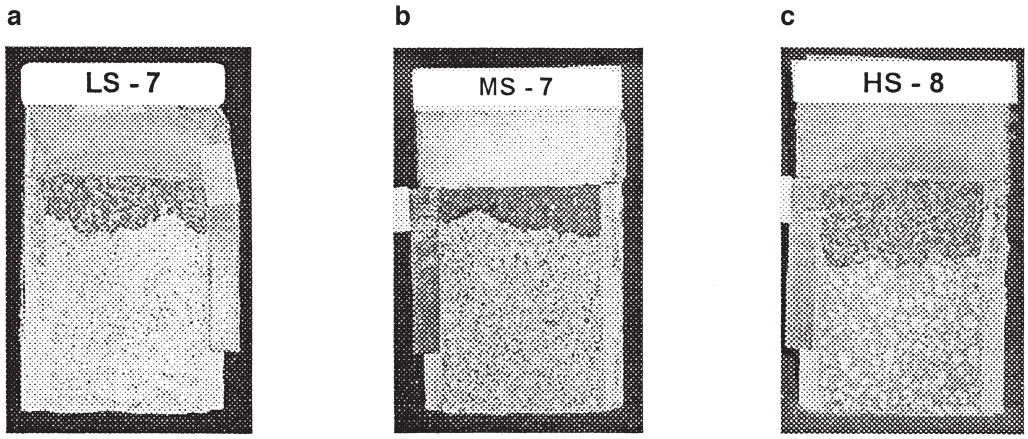

Fig. 5. The crack fronts of dyed specimens. *(a)* concrete LS, *(b)* concrete MS, *(c)* concrete HS.

2.2. Fatigue crack growth rate

Table 3 shows the results of fatigue tests. As shown in Table 3, under the same maximum load level, fatigue life decreases with increasing concrete strength. This trend was also found in tests of cylinders subjected to compressive fatigue loading [12]. As shown in Fig. 6, the relations between maximum load level P_{max}/P_u, and fatigue life N_f for the wedge-splitting tensile fatigue loading can be predicted by the same empirical model that was proposed for the compressive fatigue loading by Kim and Kim [12] as given in Eq. (7).

$$\frac{P_{max}}{P_u} = -7.6(f'_c/f_1)^{0.066}\log N_f + 126(f'_c/f_1)^{-0.025} \quad (7)$$

Table 3
Fatigue life (N_f) with concrete strength

Mixture	R (%)	P_{max}/P_u* (%)	N_f (cycles)
LS	5.9	75	42456
		75	36772
		75	18146
	13.3	85	3567
		85	2038
		85	958
MS	5.9	71	22858
		75	11590
		75	9747
	13.3	81	3147
		85	1328
		85	659
HS	5.9	71	8711
		75	5753
		75	2060
	13.3	81	1080
		85	167
		85	158

* P_u = ultimate value of monotonic loading; P_{max} = maximum value of fatigue loading.

in which N_f is fatigue life, P_{max}/P_u is maximum load level, f_c' is concrete strength of cylinder, and f_1 is 1.0 MPa.

The *P*-CMOD data measured in the fatigue test were converted to crack length and intensity range by using the CMOD compliance calibration and LEFM, respectively. The relations between fatigue crack growth a_f and number of cycles N are shown in Fig. 7, where fatigue crack growth is calculated by subtracting the initial notch length a_0 from the fatigue crack length a. In this figure, it is found that the fatigue crack growth per loading cycle depends considerably on concrete strength. This trend is attributed to the rapid fatigue failure of higher-strength concrete, as shown earlier in Table 3 and Fig. 6. Based on the data of a, N, and P, the fatigue crack growth rates were calculated by the incremental polynomial method [13].

Eq. (4) (i.e., Walker's law) is a modified form of Paris' law. If constant n is taken as zero, the effect of stress ratio vanishes, and this equation becomes Paris' law. The empirical constants m and C in Walker's law have been regarded as material constants. This is not the case, however, in con-

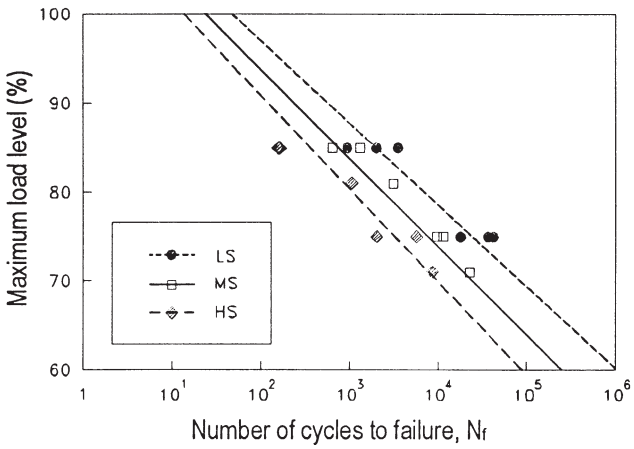

Fig. 6. Test data with $(P_{max}/P_u) - (N_f)$ empirical model.

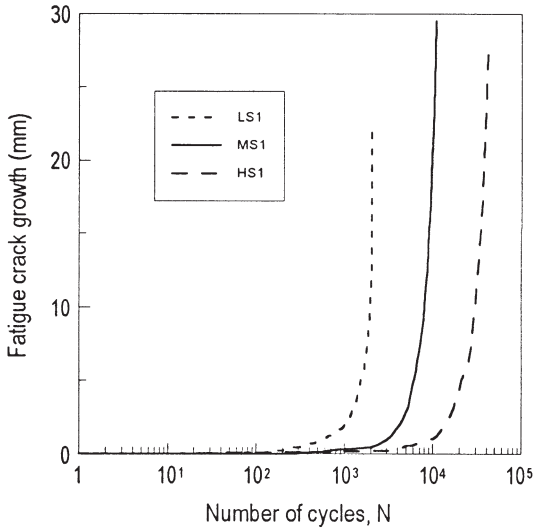

Fig. 7. The relations of the number of cycles and fatigue crack growth.

crete since the fatigue resistance of concrete varies with the strength of concrete. The constants m and C can be influenced by various parameters (i.e., fracture energy, critical stress intensity factor, tensile strength, specimen size, and the other effects). In the present study, the main parameter is concrete strength. Thus, a mathematical expression considering only strength effect was suggested. The proposed equation was based on Walker's law, in which the material constants (m, C) were regarded as the functions of concrete strength. Firstly, we assumed merely that the strength effect on C was similar to the influence of stress ratio, so $C(f_c')$ was taken as a power law. Thereafter, from the optimum fit of the present test data, the slop $m(f_c')$ was assumed to be a second-order polynomial function of concrete strength, as in Eq. (8):

$$C(f_c') = C_0 / f_c'^{k}$$
$$m(f_c') = m_0 + m_1 f_c' + m_2 f_c'^{2} \quad (8)$$

The proposed equation can be reduced to a linear regression line by plotting log da/dN vs. log ΔK, as shown in Eq. (9):

$$\log\left(\frac{da}{dN}\right) = (m_0 + m_1 f_c' + m_2 f_c'^{2})\log \Delta K + \log C_0 - k \log f_c' - n \log(1 - R) \quad (9)$$

in which C_0, k, m_0, m_1, m_2, and n are parameters determined by regression analysis, which are evaluated as follows:

1. $(m_0 + m_1 f_c' + m_2 f_c'^{2})$ is the slope of $da/dN - \Delta K$ curve of the linear relation. The influence of concrete strength is represented by parameters m_1 and m_2.
2. $[\log C_0 - k \log f_c' - n \log (1 - R)]$ is the intercept on the vertical axis of $da/dN - \Delta K$ curve. The strength effect is represented by parameter k, and the influence of stress ratio is represented by parameter n.

Eq. (9) was fitted to the test data, then the six parameters were determined as described in Eq. (10):

$$\log\left(\frac{da}{dN}\right) = (1.4 + 0.02 f_c' - 0.001 f_c'^{2})\log \Delta K + 10 - 15 \log f_c' - 20 \log (1 - R) \quad (10)$$

Parameters k and n were evaluated at 15 and 20, respectively, which expressed the trend that the empirical constant C increases with stress ratio, but decreases with increasing concrete strength. The empirical constants predicted by the proposed equation are shown in Table 4. The slope m's of concrete LS, MS, and HS were evaluated at 6.3, 9.9, and 11.6, respectively. The value of higher-strength concrete is greater than that of lower-strength concrete.

Fig. 8 shows the test data and the results of the regression analysis. For the same concrete, the slope of regression line is assumed to be the same. Slope m increases with the strength of concrete; therefore, the fatigue crack growth rate of high-strength concrete is greater than that of low-strength concrete. As a result, fatigue life should decrease with increasing concrete strength as described in Eq. (7). The intercept on the vertical axis (log C) depends on the stress ratio, and the effect can be expressed by the proposed equation.

To illustrate the accuracy of our empirical equation, Fig. 9 shows the experimental data and the predicted curves for some specimens of which the applied stress ratio is 0.059. The experimental trends were well-captured by the predicted curves, but the numerical values differed somewhat from the test data, particularly for lower strength concrete. This results from the fact that the wide scatter of fatigue life data is an inherent characteristic of concrete. Thus, the lower concrete strength is or the longer fatigue life is, the greater these differences should become. As a result, it can be seen that these differences are not significant.

3. Concluding remarks

From a fatigue crack growth test on WST specimens with three strength levels, the following conclusions can be drawn:

1. A modified Walker's law considering the strength effect was proposed. This empirical model regards the empirical constants m and C as functions of concrete strength. From the fatigue analysis, the slope m's of

Table 4
m and log C evaluated by empirical equation

	Mixture		
Constant	LS	MS	HS
m	6.3	9.9	11.6
log C			
(R: 0.059)	−11.2	−16.2	−20.6
(R: 0.133)	−10.5	−15.5	−19.9

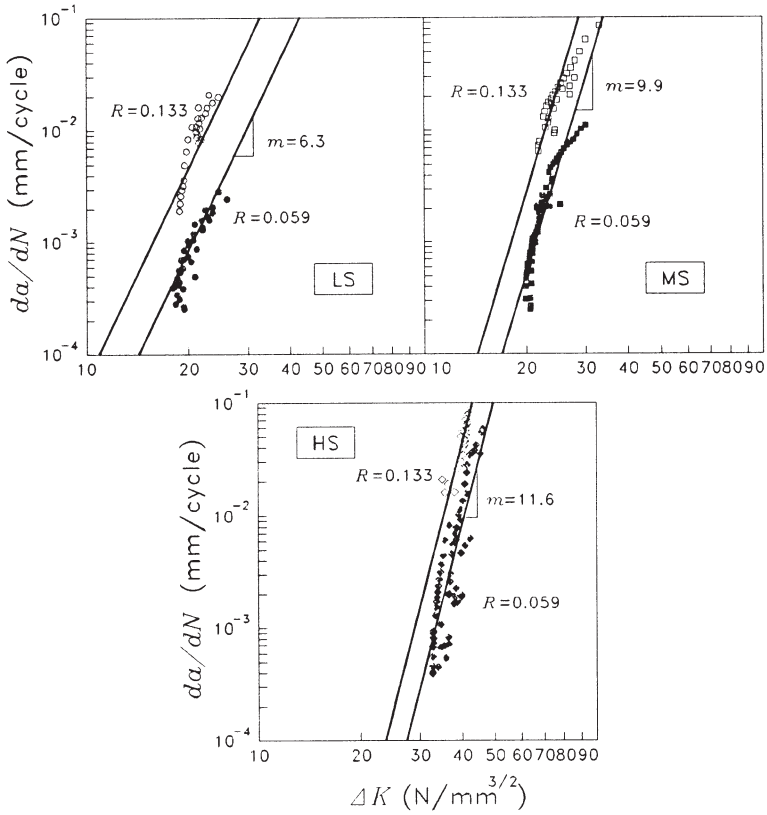

Fig. 8. Fatigue crack growth rates (test data with curves fitted).

concrete LS, MS, and HS were evaluated at 6.3, 9.9, and 11.6, respectively. Therefore, it can be concluded that the fatigue crack growth rate increases with the strength of concrete and that the fatigue life of lower-strength concrete should be longer than that of higher-strength concrete.

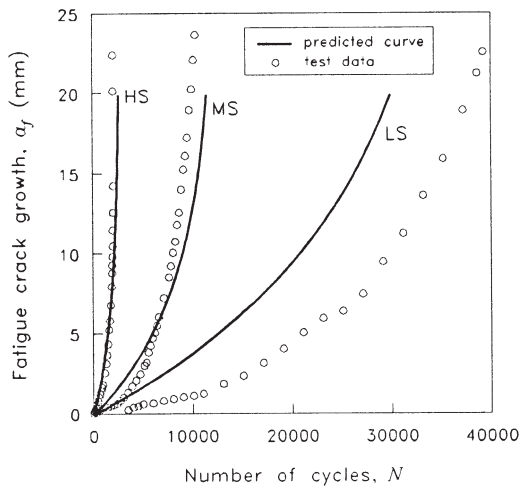

Fig. 9. The relations between the number of cycles and fatigue crack growth (test data with predicted curves).

2. On the basis of the comparison between the test data and the predicted curve of fatigue crack growth, it was found that the empirical model predicts well the crack growth trend. However, the differences present between test data and predicted numerical values are because of the inherent feature of fatigue failure (i.e., wide scatter of fatigue life data).
3. Although established from the axial compressive fatigue data, the empirical model for the $(P_{max}/P_u) - (N_f)$ relationship was found to be applicable to the data of wedge-splitting testing. This model reasonably expresses the strength dependency of fatigue life that tends to decrease with increasing concrete strength.
4. The CMOD compliances of notched specimens used for monitoring the crack length were approximately coincident with those based on LEFM and dye penetration testing. Thus, it can be concluded that the CMOD compliance calibration technique is a useful method for monitoring crack growth in wedge-splitting test.

Acknowledgment

The authors gratefully acknowledge the financial support of this work from the Korea Science & Engineering Foundations (ERC-STRESS).

References

[1] P.C. Paris, F. Erdogan, A critical analysis of crack propagation laws, Transactions of ASME Journal of Basic Engineering 85 (1963) 528–534.
[2] E.K. Walker, Effect of stress ratio during crack propagation and fatigue for 2024-t3 and 7075-t6 aluminum, in: M.S. Rosenfeld (Ed.), Effect of Environment and Complex Load History on Fatigue Life, ASTM STP 462 (1970) 81–93.
[3] M.H. Baluch, A.B. Qureshy, A.K. Azad, Fatigue crack propagation in plain concrete, SEM/RILEM International Conference on Fracture of Concrete and Rock, Houston, June 1987.
[4] P.C. Perdikaris, A.M. Calomino, Kinetics of crack growth in plain concrete, SEM/RILEM International Conference on Fracture of Concrete and Rock, Houston, June 1987.
[5] Z.P. Bazant, K. Xu, Size effect in fatigue fracture of concrete, ACI Materials J 88 (4) (1991) 390–399.
[6] Z.P. Bazant, W.F. Schell, Fatigue fracture of high-strength concrete and size effect, ACI Materials J 90 (5) (1993) 472–478.
[7] B. Zhang, Z. Zhu, K. Wu, Fatigue rupture of plain concrete analyzed by fracture mechanics, SEM/RILEM International Conference on Fracture of Concrete and Rock, Houston, June 1987.
[8] R.G. Forman, V.E. Kearney, R.M. Engle, Numerical analysis of crack propagation in cyclic-loaded structures, Transactions of ASME Journal of Basic Engineering 89 (1967) 459–464.
[9] S.E. Swartz, C.G. Go, Validity of compliance calibration to cracked concrete beams in bending, Journal of Experimental Mechanics 24 (2) (1984) 129–134.
[10] V. Slowik, G.A. Plizzari, V.E. Saouma, Fracture of concrete under variable amplitude fatigue loading, ACI Materials J 93 (3) (1996) 272–283.
[11] P.C. Perdikaris, A.M. Calomino, A. Chudnovsky, Effect of fatigue on fracture toughness of concrete, ASCE Journal of Engineering Mechanics 112 (8) (1986) 776–791.
[12] J.K. Kim, Y.Y. Kim, Experimental study of the fatigue behavior of high strength concrete, Cem Concr Res 26 (10) (1996) 1513–1523.
[13] ASTM Designation E 647-93, Standard Method for Measurement of Fatigue Crack Growth rates, 1993, pp. 569–596.